Science Advances

AAAS

advances.sciencemag.org/cgi/content/full/2/9/e1601114/DC1

Supplementary Materials for

Pattern recognition with "materials that compute"

Yan Fang, Victor V. Yashin, Steven P. Levitan, Anna C. Balazs

Published 2 September 2016, *Sci. Adv.* **2**, e1601114 (2016)
DOI: 10.1126/sciadv.1601114

This PDF file includes:

SUPPLEMENTARY INFORMATION

A. Kinetics of the BZ reaction in a polymer gel

The kinetics of the BZ reaction is described by a modification of the Oregonator model [29], formulated in terms of the dimensionless concentrations of the key reaction intermediate u ($HBrO_2$, the activator), and the oxidized metal-ion catalyst v (Ru^{3+} in the case considered here). The modified model [9,10] accounts for the dependence of the BZ reaction rates on the volume fraction of polymer ϕ, and on the total concentration of catalyst grafted to the network. The reaction rates F_{BZ} and G_{BZ} in eqs. (1) and (2) are determined as follows

$$F_{BZ}(u,v,\phi) = (1-\phi)^2 wr - u^2 - (1-\phi) f v \frac{u - q(1-\phi)^2}{u + q(1-\phi)^2} \qquad \text{(S1)}$$

$$G_{BZ}(u,v,\phi) = \varepsilon_{BZ} [(1-\phi)^2 wr - (1-\phi) v] \qquad \text{(S2)}$$

The reaction rates depend on the dimensionless concentrations of the reduced catalyst Ru^{2+} and the radical BrO_2^* denoted by r and w, respectively [S2]. The concentration r is calculated as $r = c_{Ru} \phi_0^{-1} \phi - v$, where c_{Ru} and ϕ_0 are the catalyst concentration and volume fraction of polymer in the undeformed gel, respectively. The concentration of the radical w is found as $w = \mu_{BZ} (r^2 + 2u/\mu_{BZ})^{1/2} - \mu_{BZ} r$, where μ_{BZ} is a dimensionless parameter [S2]. Finally, the stoichiometric factor f and the dimensionless parameters q and ε_{BZ} have the same meaning as in the original Oregonator model [29].

We assume that the chemical composition of the BZ substrate and the volume fraction of polymer in the undeformed gel are the same as used in the experiments described in ref. [10], so

the corresponding dimensionless parameters are estimated to be $\varepsilon_{BZ} = 0.212$, $q = 9.52 \times 10^{-5}$, $\mu \approx 7 \times 10^{2}$, and $\phi_0 = 0.16$. The stoichiometric parameter f and the catalyst content c_{Ru} are the adjustable parameters in the study, and we assume them to be $f = 1$ and $c_{Ru} = 3$.

B. Osmotic pressure of the polymer in a gel

The osmotic pressure of the polymer in gel is calculated according to the Flory-Huggins theory

$$\pi_{FH} = -[\phi + \log(1-\phi) + \chi(\phi)\phi^2] \tag{S3}$$

Here, $\chi(\phi)$ describes the polymer-solvent interactions. It is calculated as $\chi(\phi) = 0.338 + 0.518\phi$, which is known to describe the PNIPAAm-water interaction at $20^{\circ}C$ [30]. Equation (S3) does not include the interaction between the BZ catalyst and solvent; the latter is taken into account by the second term on the right-hand-side of eq. (3).

C. Properties of a bending piezoelectric bimorph plate

The coefficients m_{11}, m_{12}, and m_{22} in eqs. (4) and (5) that describe the behavior of a bending piezoelectric bimorph plate are given by the following equations [14]

$$m_{11} = \frac{(L_p / h_p)^3}{2 w_p E} \tag{S4}$$

$$m_{12} = \frac{3}{4} d_{31} (L_p / h_p)^2 \tag{S5}$$

$$m_{22} = 2 w_p \varepsilon_{33} (1 - k^2 / 4)(L_p / h_p) \tag{S6}$$

Here, L_p, w_p, and h_p are the respective length, width, and layer thickness of the piezoelectric bimorph plate; E, d_{31}, and ε_{33} are the Young's modulus, piezoelectric constant, and dielectric

constant of the piezoelectric material, respectively. Finally, $k = (d_{31}^2 E / \varepsilon_{33})^{1/2}$ is the electromechanical coupling factor characterizing the piezoelectric material.

The piezoelectric bimorph plate dimensions are taken to be $L_p = w_p = 1\text{mm}$, and $h_p = 10\,\mu\text{m}$. The plate is assumed to be fabricated from polarized Lead-Zirconate-Titanate (PZT) ceramics. A typical PZT ceramic has a Young's modulus of $E = 50\,\text{GPa}$; typical values for the other parameters are $d_{31} = -1.5\times10^{-10}\,\text{mV}^{-1}$ and $\varepsilon_{33} = 1.8\times10^{3}\varepsilon_0$, where $\varepsilon_0 = 8.85\,\text{pF m}^{-1}$ is the dielectric constant of the vacuum [24]. In our calculations, we use the latter values of E and ε_{33}, and a twofold greater value for the piezoelectric constant (setting $d_{31} = -3\times10^{-10}\,\text{mV}^{-1}$), which can be achieved in PZT through sophisticated processing methods [25,26].

D. Procedure used to map phase dynamics to $0 \le \varphi \le 0.5$

The phase of oscillation is defined as $0 \le \varphi \le 1$. In order to plot the phase dynamics within the range $[0,0.5]$, the phase differences within the range $[0.5,1]$ are mapped onto $[0,0.5]$, as if the entire plot is folded in half. The latter procedure is illustrated in the plot below:

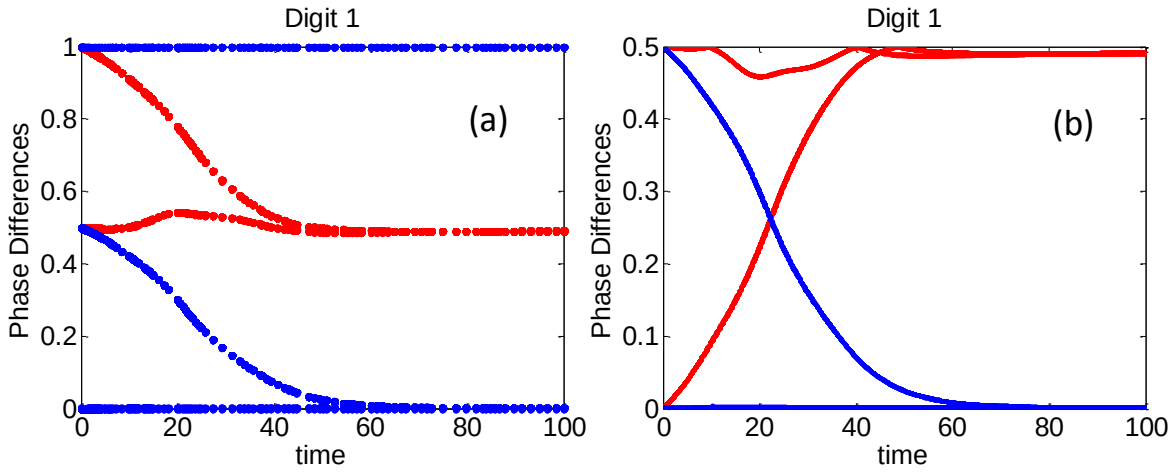

fig. S1. The phase differences plotted in the range (**a**) [0,1] and (**b**) [0, 0.5]. The BZ-PZ oscillators with the force polarity of $+1$ (white pixels in the stored image) are represented by the blue color, and the ones with force polarity of -1 (black pixels) are labeled with red.

E. Stability of the synchronization mode

In this section, we use the linear stability approach to show that the synchronization mode used for the pattern recognition is stable. We consider a system of n serially connected BZ-PZ oscillator units; n_1 of these units have force polarities of +1 and the remaining $n_2 = n - n_1$ units have force polarities of -1. The equation of phase dynamics, eq. (8), is invariant under a renumbering of the units so we assign the polarity $+1$ to the units $i = 1, 2, \ldots, n_1$, and the polarity -1 to the units $j = n_1 + 1, n_1 + 2, \ldots, n$. The application of eq. (8) to the two groups of units gives the following equations of phase dynamics

$$\kappa^{-1} d\varphi_i/dt = \mathrm{H}(0) - n^{-1} \sum_{k=1}^{n_1} \mathrm{H}(\varphi_k - \varphi_i) + n^{-1} \sum_{l=n_1+1}^{n} \mathrm{H}(\varphi_l - \varphi_i) \tag{S7}$$

$$\kappa^{-1} d\varphi_j/dt = \mathrm{H}(0) + n^{-1} \sum_{k=1}^{n_1} \mathrm{H}(\varphi_k - \varphi_j) - n^{-1} \sum_{l=n_1+1}^{n} \mathrm{H}(\varphi_l - \varphi_j) \tag{S8}$$

We assume that upon synchronization, the oscillators are synchronized in-phase within each group, and that the difference in phase of oscillation between these two groups is ψ. By

substituting $\varphi_i = \nu t$ and $\varphi_j = \nu t + \psi$ to eqs. (S7) and (S8), we obtain the following equations for the constant shift in the frequency of oscillation ν and the phase difference ψ that characterize the state of synchronization

$$n\kappa^{-1}\nu = n_2[\mathrm{H}(0) + \mathrm{H}(\psi)] \tag{S9}$$

$$n\kappa^{-1}\nu = n_1[\mathrm{H}(0) + \mathrm{H}(1-\psi)] \tag{S10}$$

Equation (S10) is written with taking into account that the connection function $\mathrm{H}(\theta)$ is periodic so $\mathrm{H}(-\psi) = \mathrm{H}(1-\psi)$. Subtraction of eq. (S10) from eq. (S9) yields the equation for the phase difference

$$(n_2 - n_1)\,\mathrm{H}(0) + n_2\,\mathrm{H}(\psi) - n_1\,\mathrm{H}(1-\psi) = 0 \tag{S11}$$

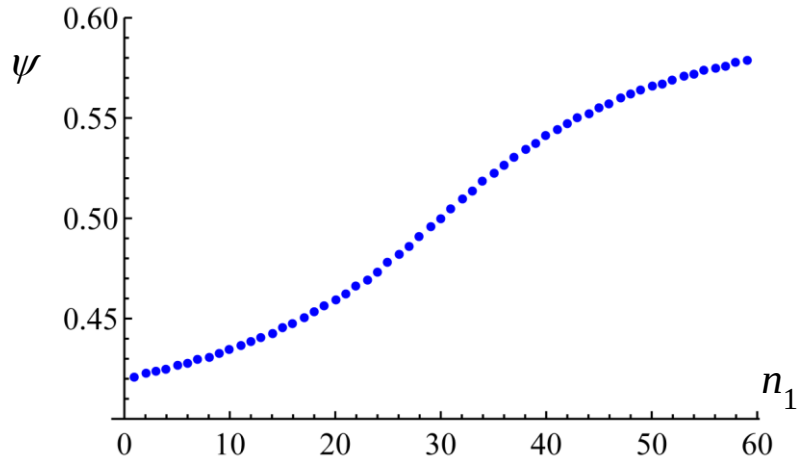

fig. S2. The phase difference ψ between the two groups of oscillators obtained by numerical solution of eq. (S11) at $n = 60$.

The connection function $\mathrm{H}(\theta)$ is known (see Fig. 13) so the phase difference ψ can be found by numerical solution of eq. (S11). Figure S2 shows the calculated values of ψ as a function of n_1 at $n = 60$.

In order to study the stability of the synchronization state, we introduce the phase difference between the oscillator $i = 2,\ldots,n$ and the oscillator 1, $\theta_i = \varphi_k - \varphi_1$, and use eqs. (S7) and (S8) to obtain the equations for θ_i. For $i = 2,\ldots,n_1$, the equation is

$$n\kappa^{-1} d\theta_i/dt = -[\mathrm{H}(-\theta_i) - \mathrm{H}(\theta_i)] - \sum_{\substack{k=2 \\ k\neq i}}^{n_1} [\mathrm{H}(\theta_k - \theta_i) - \mathrm{H}(\theta_k)] + \sum_{l=n_1+1}^{n} [\mathrm{H}(\theta_l - \theta_i) - \mathrm{H}(\theta_l)] \tag{S12}$$

and for $j = n_1 + 1, n_1 + 2,\ldots,n$, the obtained equation is

$$n\kappa^{-1} d\theta_j/dt = \mathrm{H}(-\theta_j) - \mathrm{H}(\theta_j) + \sum_{k=2}^{n_1} [\mathrm{H}(\theta_k - \theta_j) + \mathrm{H}(\theta_k)] - \sum_{\substack{l=n_1+1 \\ l\neq j}}^{n} [\mathrm{H}(\theta_l - \theta_j) + \mathrm{H}(\theta_l)] \tag{S13}$$

Linearization of eqs. (S12) and (S13) around the steady state, $\theta_i = \bar{\theta}_i + \delta\theta_i$, where $\bar{\theta}_i = 0$ for $i = 2,\ldots,n$ and $\bar{\theta}_j = \psi$ for $j = n_1 + 1, n_1 + 2,\ldots,n$, yields the following two respective equations for the phase perturbations

$$n\kappa^{-1} d\delta\theta_i/dt = a_1 \delta\theta_i \tag{S14}$$

$$n\kappa^{-1} d\delta\theta_j/dt = a_2 \delta\theta_j + b\sum_{k=2}^{n_1} \delta\theta_k - c\sum_{l=n_1+1}^{n} \delta\theta_l \tag{S15}$$

In eqs. (S14) and (S15), a_1, a_2, b, c are the numerical coefficients defined as

$$a_1 = n_1 \mathrm{H}'(0) - n_2 \mathrm{H}'(\psi) \tag{S16}$$

$$a_2 = n_2 \mathrm{H}'(0) - n_1 \mathrm{H}'(1-\psi) \tag{S17}$$

$$b = \mathrm{H}'(0) + \mathrm{H}'(1-\psi) \tag{S18}$$

$$c = \mathrm{H}'(0) + \mathrm{H}'(\psi) \tag{S19}$$

where the prime denotes the derivative of the connection function H with respect to phase. The synchronization state is stable if all the eigenvalues of the matrix $\mathbf{M}$

$$\mathbf{M} = \begin{bmatrix} \mathbf{A}_1 & \mathbf{0} \\ \mathbf{B} & \mathbf{A}_2 \end{bmatrix} \tag{S20}$$

are negative. The matrix $\mathbf{M}$, eq. (S20), has a block structure, where $\mathbf{A}_1$ is a $(n_1 - 1) \times (n_1 - 1)$ diagonal matrix, $[\mathbf{A}_1]_{ij} = a_1 \delta_{ij}$, $\mathbf{A}_2$ is a $(n_2 \times n_2)$ matrix with the elements $[\mathbf{A}_2]_{ij} = a_2 \delta_{ij} - c$, $\mathbf{B}$ is a $n_2 \times (n_1 - 1)$ matrix with all elements equal to b, $[\mathbf{B}]_{ij} = b$, and $\mathbf{0}$ is a $(n_1 - 1) \times n_2$ block filled with zeroes.

Due to the block structure of eq. (S20), the set of eigenvalues of the matrix $\mathbf{M}$ consists of the eigenvalues of the matrices $\mathbf{A}_1$ and $\mathbf{A}_2$. The matrix $\mathbf{A}_1$ is diagonal with all the elements equal to a_1; hence, all the eigenvalues of $\mathbf{A}_1$ are equal to a_1. The matrix $\mathbf{A}_2$ is a circulant matrix. By definition [31], a $(n \times n)$ matrix $\mathbf{C}$ is circulant if each row is obtained by a cyclic shift to the right of the row above it

$$\mathbf{C} = \begin{bmatrix} c_1 & c_2 & \dots & c_n \\ c_n & c_1 & \dots & c_{n-1} \\ \vdots & \vdots & \vdots & \vdots \\ c_2 & c_3 & \dots & c_1 \end{bmatrix}$$

It is known that the eigenvalues λ_j, $j = 1, 2, \dots, n$, of the matrix $\mathbf{C}$ are [31]

$$\lambda_j = \sum_{k=1}^{n} c_k \exp\left(\frac{2\pi i}{n} (k-1)(j-1) \right) \tag{S21}$$

where $i = \sqrt{-1}$ is the imaginary unit. Applying eq. (S21) to the matrix $\mathbf{A}_2$, we conclude that it possesses two distinct eigenvalues equal to a_2 and $a_2 - n_2 c$. During the calculations, it is taken into account that

$$\sum_{k=1}^{n} \exp\left(\frac{2\pi i}{n} (k-1)(j-1) \right) = n \delta_{j1}$$

Thus, the matrix $\mathbf{M}$ has the three distinct eigenvalues $\{a_1, a_2, a_2 - n_2 c\}$, which depend on the connection function H, the number of oscillators in the system n, and on the set of force polarities n_1 and $n_2 = n - n_1$ (see eqs. (S11), (S16), (S17), and (S19). Numerical calculations show that all the eigenvalues are negative at $n = 60$ and $n_1 = 1, 2, \ldots, 59$. Therefore, the synchronization mode used for the pattern recognition is stable.

F. Complete set of results for Test 3

In the paper, figs. 11 and 12 show the results of Test 3 for only the digitized images '1', '3', '5', and '7'. Figures S3 and S4 present the complete set of results that includes the digitized images from '0' to '9'.

The decrease in the accuracy of the pattern recognition with an increase in the number of flipped pixels (i.e., noise) is less drastic if the number of pixels that are flipped between successive simulations is incremented by a small amount. In particular, in Fig. 11 and 12, the number of flipped bits between successive simulations is increased by five. Figure S5 shows the accuracy of recognizing the digit "7" when only one pixel is flipped in each subsequent simulation. Notably, the plot shows a smooth decrease in accuracy.

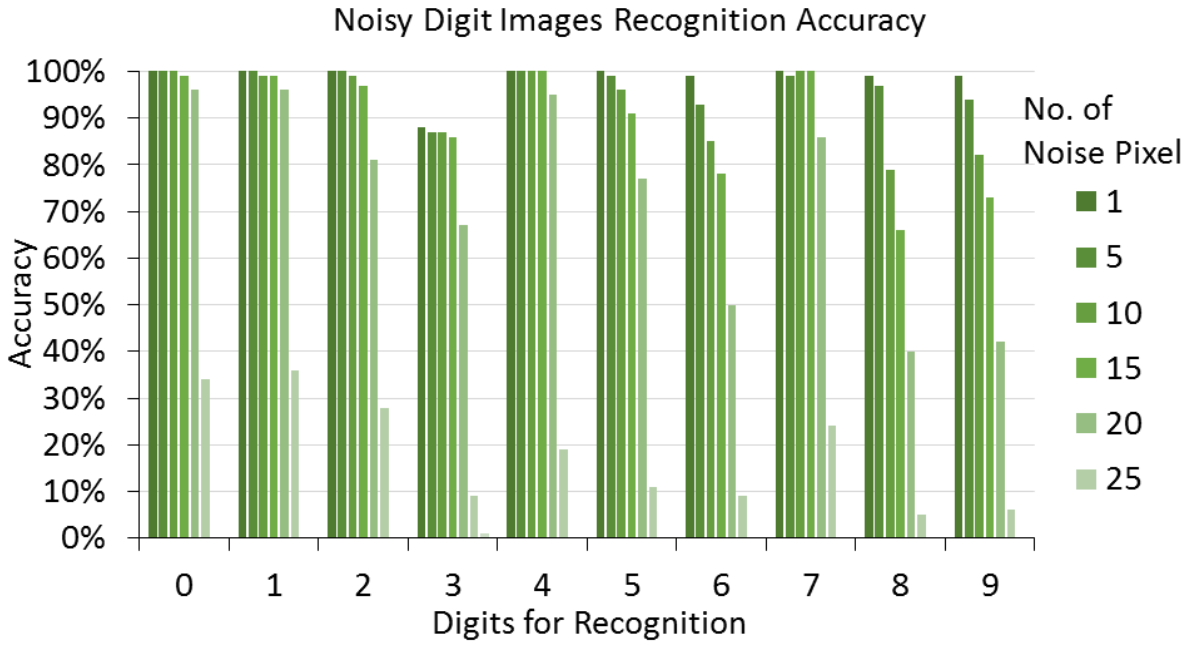

fig. S3. The accuracies of the recognition test 3 for the input patterns of all 10 digits distorted with various levels of noise. The bars are colored according the noise level. The horizontal axis indicates the input patterns.

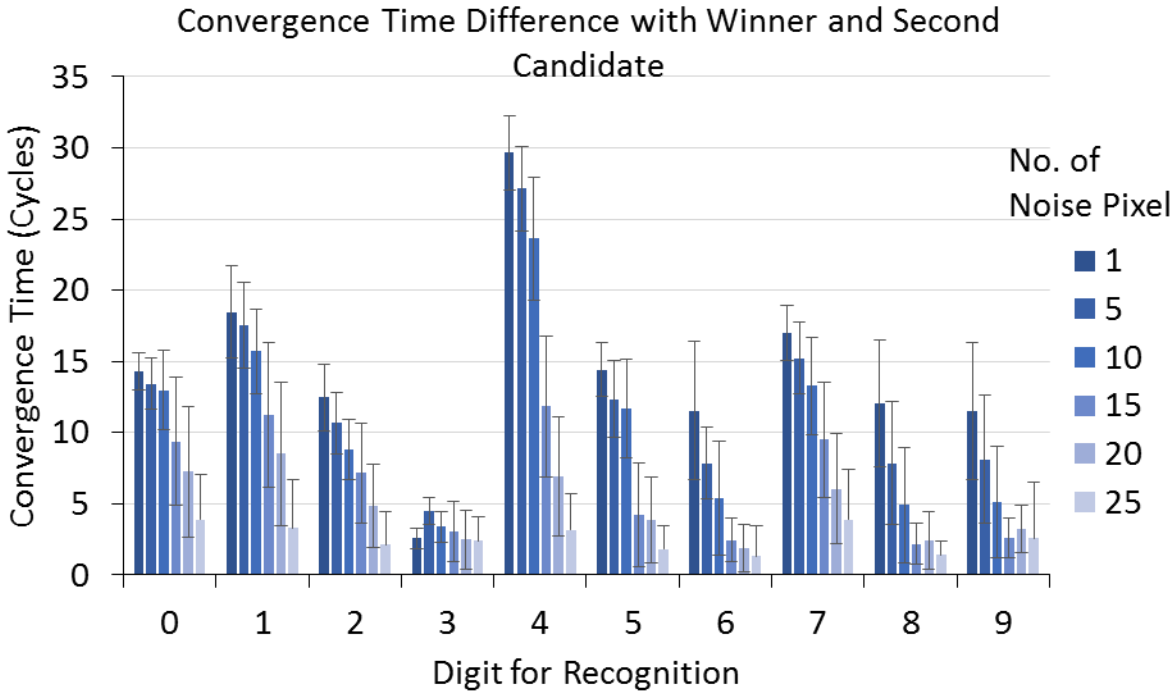

fig. S4. The height of the bars represents the average convergence time difference between the winner and the runner-up in all the hit cases in test 3. The error bars show the standard deviation obtained for each bar. The results indicate how fast the correct, recognized winner leads the runner-up. Other notations are the same as in fig. S3.

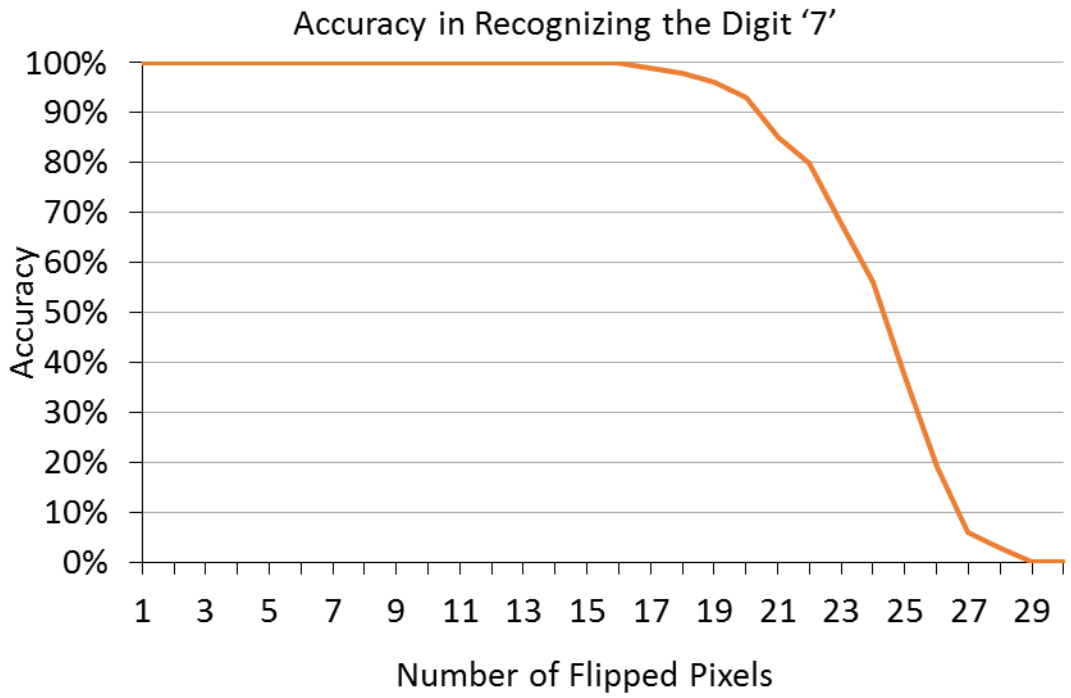

fig. S5. The accuracy in recognizing the digit "7" as a function of the number of flipped pixels in the case where 60 pixels are used to represent the digit.

G. The effect of gel heterogeneities on synchronization

Within our model for the BZ-PZ system, it is assumed that all the BZ-PZ units are chemically and physically identical. The effect of variations in the properties of the individual oscillators, however, can be estimated within the phase dynamics approach. Specifically, we consider a network of BZ-PZ units where the periods of the free-running oscillations vary around T_0 due to heterogeneities among the units. The dynamics of this system is described by the following generalization of eq. (8)

$$d\varphi_i/dt = \Delta T_i / T_0 + \kappa\, \mathrm{H}(0) - \kappa\, n^{-1} \sum_{j=1}^{n} \varepsilon_i \varepsilon_j\, \mathrm{H}(\varphi_j - \varphi_i)$$

where $\Delta T_i = T_i - T_0$ is the detuning of oscillator i.

We assume that the relative variation of the period of oscillation, $\Delta T / T_0$, is a uniformly distributed random value within the interval $[-\sigma, \sigma]$, and perform simulations at various values of the distribution width σ. Figure S6 shows the results of the simulation for the evolution of the input pattern corresponding to the distorted digit "1" towards the stored pattern "2" (see Fig. 4, third row) at four values of σ. When σ equals 0.001κ and 0.002κ, the synchronization dynamics is similar to that in the case of the identical oscillators. The only effect of the heterogeneity is a "widening" of the two final states of synchronization, i.e., the phases are

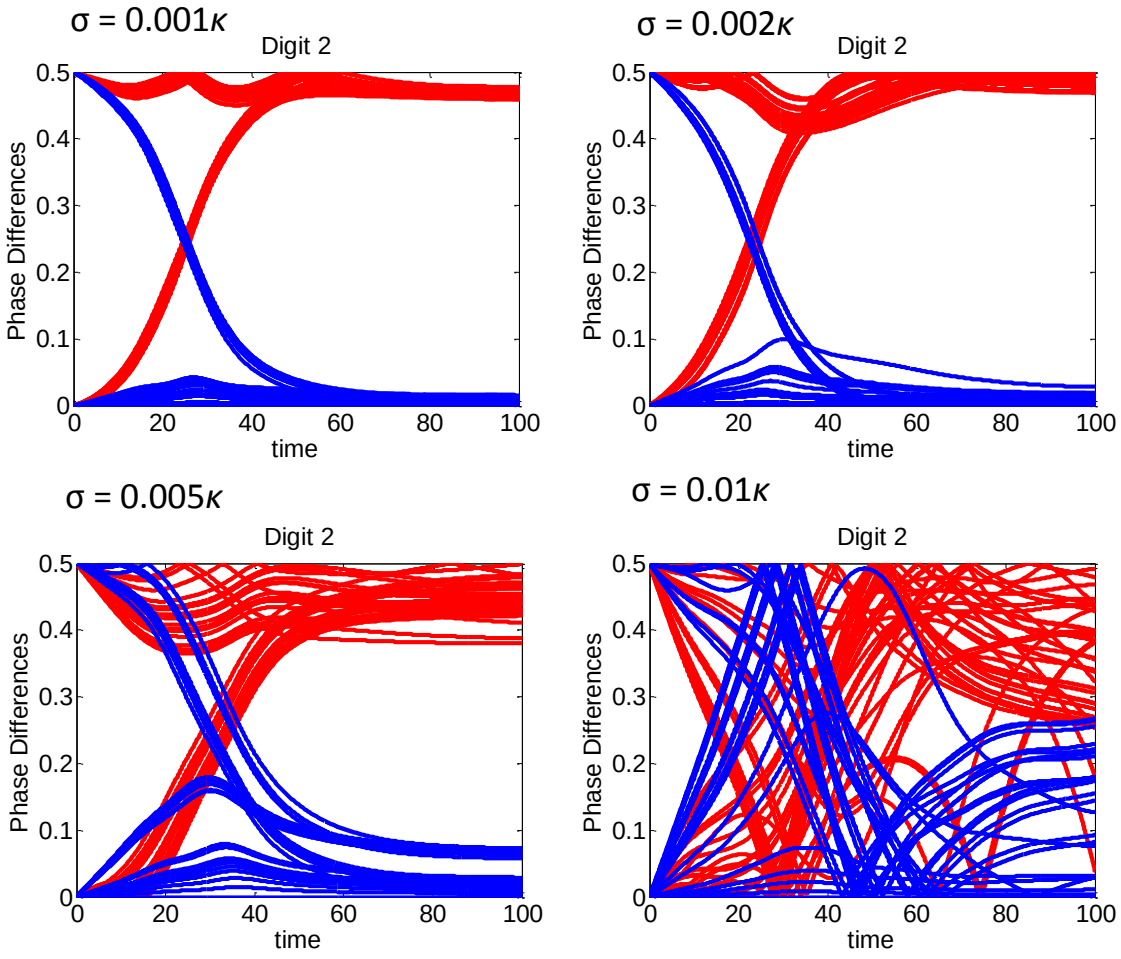

fig. S6. The phase dynamics for the uniform distribution $\Delta T / T_0 \in [-\sigma, \sigma]$ for various values of σ.

grouped within narrow bands around the phase differences 0 and 0.5. A further increase of the distribution width to $\sigma = 0.005\kappa$ makes the recognition problematic, and the recognition is impossible at $\sigma = 0.01\kappa$.

The criterion of convergence used for the pattern recognition should be adjusted depending on the magnitude of variations in $\Delta T / T_0$. The latter observation is evident from fig. S7, which shows an increase in the scattering of the convergence times resulting from an increase in the distribution width σ from $1\times10^{-4}\kappa$ to $2\times10^{-3}\kappa$. Here, we set the convergence threshold to 0.1 (each oscillator's phase is within 10% of the group average), which is 10 times greater than the value used for the studies described in the main text.

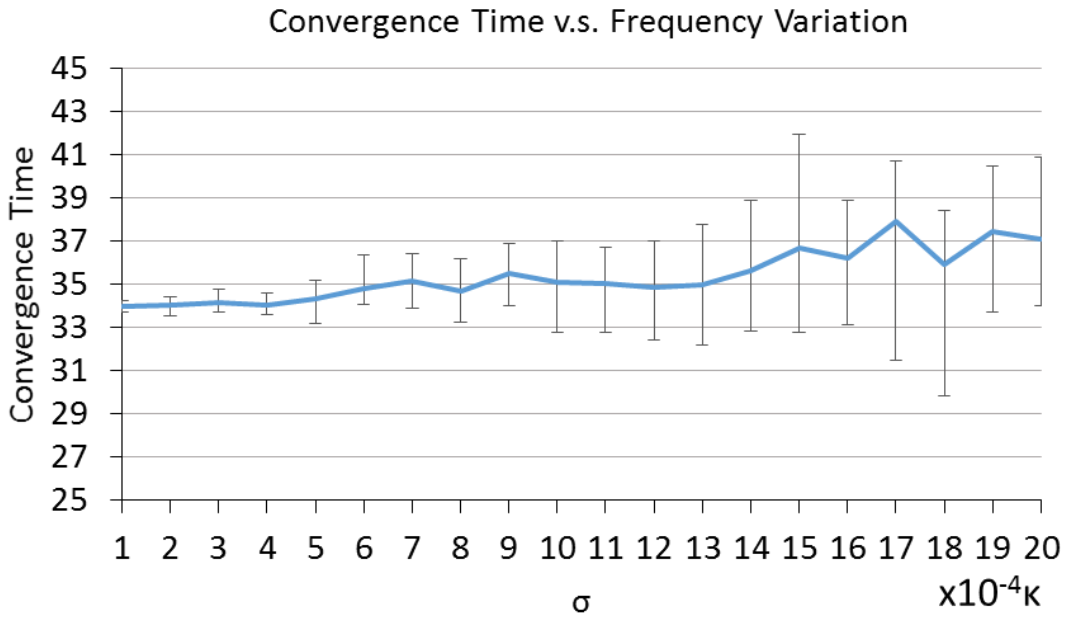

fig. S7. The convergence time at random $\Delta T / T_0 \in [-\sigma, \sigma]$ as a function of the distribution width σ. The convergence threshold is 0.1.